

Unveiling the interaction of protein fibrils with gold nanoparticles by plasmon enhanced nano-spectroscopy

Angela Capocefalo,^{a,b} Tanja Deckert-Gaudig,^{c,d} Francesco Brasili^a, Paolo Postorino^a and Volker Deckert^{*c,d,e}

This is the pre-peer reviewed version of the following article: *Nanoscale*, 2021, **13**, 14469, which has been published in final form at <https://doi.org/10.1039/D1NR03190B>.

The development of various degenerative diseases is suggested to be triggered by the uncontrolled organisation and aggregation of proteins into amyloid fibrils. For this reason, there are ongoing efforts to develop novel agents and approaches, including metal nanoparticle-based colloids, that dissolve amyloid structures and prevent pathogenic protein aggregation. In this contribution, the role of gold nanoparticles (AuNPs) in degrading amyloid fibrils of the model protein lysozyme is investigated. The amino acid composition of fibrils surfaces before and after the incubation with AuNPs is determined at the single fibril level by exploiting the high spatial resolution and sensitivity provided by tip-enhanced and surface-enhanced Raman spectroscopies. This combined spectroscopic approach allowed to reveal the molecular mechanisms driving the interaction between fibrils and AuNPs. Our results provide an important input for the understanding of amyloid fibrils and could have a potential translational impact on the development of strategies for the prevention and treatment of amyloid-related diseases.

Introduction

Misfolding and aggregation phenomena of specific proteins are often associated with the development of various diseases, including Alzheimer's, Parkinson's diseases, and type II diabetes¹. The process, known as fibrillation, involves the loss of the native folding of proteins and their self-assembly into fibrous, insoluble aggregates, so-called amyloid fibrils. In the last decades, numerous studies have pointed out that, for most proteins, fibrillation is a multi-step process, starting with the formation of small protein aggregates. The cooperative association of those so-called prefibrillar oligomers through non-covalent interactions produces amyloid fibrils with a typical diameter of tens of nanometres and a length that can reach several micrometres².

Understanding the mechanisms of fibrillation and developing agents capable of preventing or reversing undesired protein aggregation is pivotal to new therapeutic approaches for amyloid-related diseases. To date, polyphenols, mostly naturally occurring organic molecules, have been identified as blocking factors in amyloidogenesis³⁻⁵. Recently, there has been growing interest in the use of biocompatible inert metal nanoparticles (NPs)⁶⁻⁸, both as inhibitors of protein aggregation⁹⁻¹¹ and folding assistants, analogous to molecular chaperones¹². Consequently, the elucidation of the underlying molecular mechanisms of NPs-fibrils interaction is a crucial point for the actual therapeutic employment of NPs. So far, little is known about the influence of NPs on the stability of amyloid

fibrils and on the biological effect resulting from the interactions¹³⁻¹⁵.

A promising approach to obtain detailed insights at the single amino acid level is provided by plasmon-enhanced spectroscopies, which allow a highly sensitive characterisation of materials¹⁶. These techniques take advantage of the optical properties of plasmonic materials, such as noble metal NPs, that confine strong electromagnetic fields in spatial regions with dimensions well below the diffraction limit¹⁷. The light confinement generates an enormous enhancement of the Raman signal intensity of analytes located close (within a few nanometres) to the plasmonic surface and consequently excludes the signal from other regions.

Well known sensitive enhanced spectroscopies that are nowadays broadly employed in biosensing are based on Raman scattering, namely surface-enhanced Raman spectroscopy (SERS)^{13,16,18} and tip-enhanced Raman spectroscopy (TERS)¹⁹⁻²¹. The latter combines the molecular specificity and huge signal enhancement of SERS with the nanometre spatial resolution of scanning probe microscopy²². The key component of TERS is a plasmonic-active tip that simultaneously acts as Raman signal amplifier and topography scanner. The exceptional spatial resolution of this technique has led to unique results in mapping protein fibrils with single amino acid resolution^{23,24} and even in the sequencing of nucleic acids^{25,26}.

The present study gives insight into the interactions between lysozyme fibrils and gold NPs (AuNPs). Lysozyme was chosen as an amyloidogenic model protein, since it is interesting from a biomedical point of view: its misfolding and accumulation of fibrils in organs is associated with hereditary non-neuropathic systemic amyloidosis²⁷. Moreover, lysozyme fibrillation has already been characterised by optical and near-field microscopies as well as with conventional spectroscopic techniques^{28,29}. AuNPs are currently broadly tested in nanomedicine due to their good biocompatibility and their flexible optical properties which make them well-suited for chemical sensing and drug delivery³⁰⁻³².

^a Dipartimento di Fisica, Sapienza Università di Roma, P. le Aldo Moro 5, Roma, Italy.

^b CNR-ISC, Istituto dei Sistemi Complessi, Università Sapienza, Piazzale Aldo Moro 5, 00185 Roma, Italy.

^c Leibniz Institute of Photonic Technology (IPHT), Albert-Einstein-Str. 9, 07745 Jena, Germany.

^d Institute of Physical Chemistry and Abbe Center of Photonics, Friedrich-Schiller-University Jena Helmholtzweg 4, 07743 Jena, Germany.

^e Institute of Quantum Science and Engineering, Texas A&M University, College Station, TX 77843-4242, USA

E-mail: volker.deckert@uni-jena.de

Electronic Supplementary Information (ESI) available.

See DOI: 10.1039/D1NR03190B.

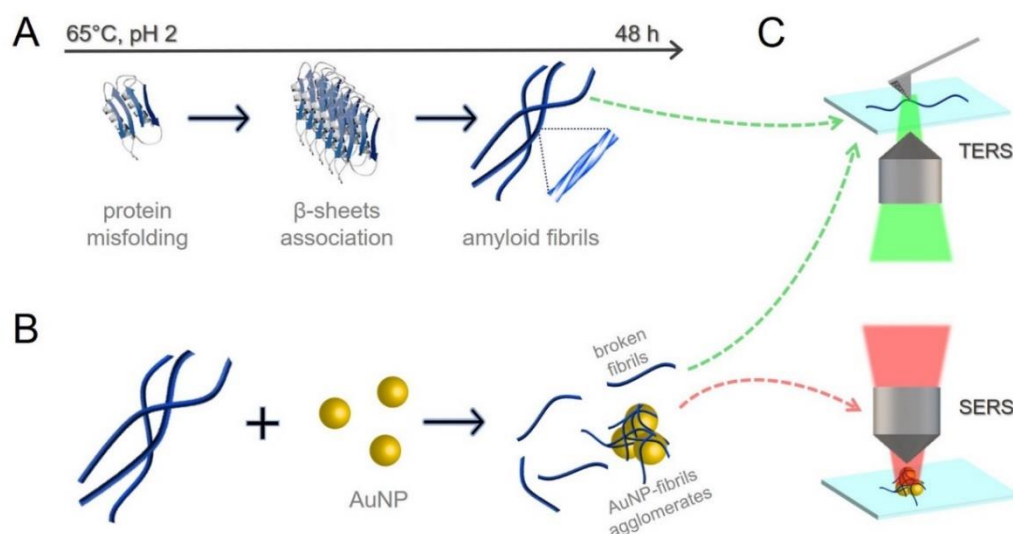


Figure 1. Sketch of the different experiments performed in this contribution: (A) lysozyme fibrillation, induced by thermal denaturation in acidic solution (pH 2); (B) study of the interaction between mature fibrils and fibril fragments and AuNPs using SERS; (C) TERS experiments on single lysozyme fibrils in the presence of AuNPs and without.

In the present contribution, complementary TERS and SERS experiments were performed as sketched in Fig. 1. TERS provides information about the amino acid composition of fibril surfaces before and after the incubation with AuNPs, while SERS intrinsically probes the signal from the protein region which is chemically bound to the gold nanoparticles. Besides providing a deep nano-spectroscopic characterisation of the amyloid structures, this approach suggests novel interaction mechanisms between AuNPs and fibrils.

Results and discussion

Morphological and nano-spectroscopic characterisation of lysozyme fibrils

Lysozyme fibrillation was performed following the protocol given in the experimental section. The morphology of the different aggregates grown in the process was imaged with an atomic force microscopy (AFM). The fibrillation kinetic was investigated for 48 h and aliquots of the solution were collected at given time points and deposited onto pre-cleaned glass slides. The different steps of the fibrillation are characterised by the formation of pre-fibrillar intermediates and are in agreement with earlier results reported in the literature³³. After 48 h thermal treatment, the sample solution changed to a soft transparent gel. Concurrently, mature fibrils were observed in the topography images in the AFM measurements. Representative images of mature fibrils showing an elongated structure extended for tens of microns are shown in Fig. 2A. Further representative topography images acquired at varying incubation time points are given in Fig. S1 in the Supplementary Information.

From Fig. 2B it is evident that it is possible to distinguish single thin protofilaments from mature fibrils assembled in intertwined structures. The height profile in Fig. 2C allows an

estimation of the average height of ~ 5 nm and a width of ~ 30 nm for mature fibrils. It is important to note that the width does not describe the actual width of the fibrils but is a convolution of the tip shape and the fibril. The periodicity of the intertwining of 105.2 ± 3.5 nm was obtained by analysing height profiles along the fibril axis (see Fig. 2D). According to literature³⁴, and in agreement with previous studies on hen egg white lysozyme³⁵, such periodicity is characteristic for structures composed of four intertwined protofilaments.

The TERS results from the experiments of lysozyme fibrils are summarised in Fig. 3. Fig. 3A shows the AFM topography image and the consecutively acquired spectra along the fibril main axis. The tentative assignment of the main bands of the spectra, based on previous TERS and Raman studies on protein and protein fibrils^{5,23,36,37}, is reported in Table 1. The propensity of the selected amino acids on the surface of mature fibrils was calculated from the ratio of the number of spectra in which their specific spectral markers were identified and the total number of spectra analysed (see propensity histogram in Fig. 3B.). In agreement with standard Raman spectra of peptides and proteins, the most intense spectral features in the TERS spectra of lysozyme fibrils are the bands of aromatic side chain modes. The amino acid sequence of lysozyme³⁸ is based on 129 amino acids, including 12 aromatic moieties: three phenylalanine (Phe), three tyrosine (Tyr) and six tryptophan (Trp). In general, for amino acids with a single aromatic ring such as Tyr and Phe, the ring breathing modes at $825\text{--}855\text{ cm}^{-1}$ and $997\text{--}1014\text{ cm}^{-1}$, respectively, are used as marker bands³⁶. Since the latter band may overlap with the Trp indole ring breathing mode at $1004\text{--}1010\text{ cm}^{-1}$,³⁶ an unambiguous assignment of Trp is only possible by considering a combination of bands associated with the indole ring system³⁹. Specifically, these are the lower frequency indole breathing mode at $740\text{--}770\text{ cm}^{-1}$ and the indole C=C stretching vibrations at $1332\text{--}1335\text{ cm}^{-1}$ and $1533\text{--}1552\text{ cm}^{-1}$.

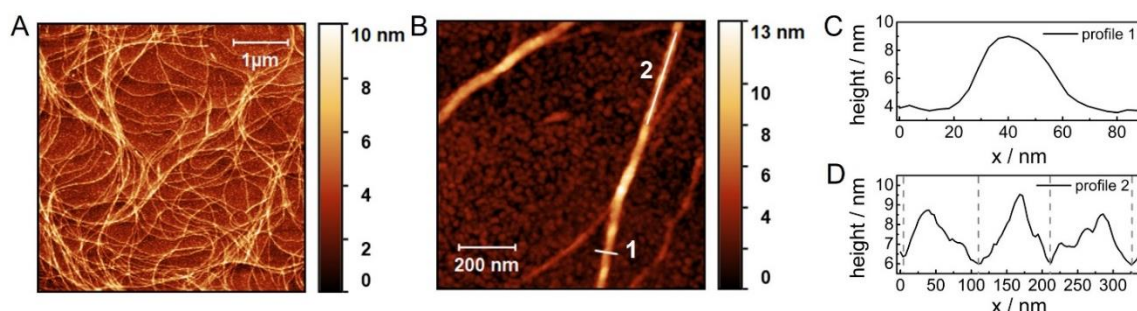


Figure 2. (A) AFM topography overview image of mature lysozyme fibrils formed after 48 h of thermal treatment. (B) Detailed AFM topography image of single protofilaments and fibrils. Line 1 and 2 indicate where the height profiles shown in panel (C) and (D) were measured. In panel D, the vertical dashed lines point to the periodicity of the intertwinement along the main fibril axis.

Several marker bands of cysteine (Cys) are detected in the low frequency region, below 680 cm^{-1} , indicating a $\sim 70\%$ propensity on the fibrils surface. In the spectra along the fibril, the positions of these bands vary due to the presence of different conformers²³. In particular, bands in the $530\text{--}550\text{ cm}^{-1}$ range can be assigned to disulphide bridges⁴⁰ and are detected in 27.2% of the TERS spectra. Since two Cys residues are linked by a S-S bond, the proportion of Cys involved in S-S bonds was estimated to 56%. Nevertheless, the spectral region corresponding to S-S bonds extends down to 510 cm^{-1} ,³⁶ and is partially obscured by the strong signal at 520 cm^{-1} of the silver-coated silicon TERS tip. Therefore, the actual number of spectral markers corresponding to S-S bonds could be underestimated.

In the folded state of lysozyme, eight Cys residues form four disulphide bridges, which contribute to a robust globular structure of the native protein. Even though the partial denaturation of the protein is assumed in the preliminary step of fibrillation, it is still under debate whether the rupture of all disulphide bridges is a necessary parameter⁴¹. Our analysis points out that at least a part of the native disulphide bridges is preserved without preventing the fibrillation/aggregation of

lysozyme. Similarly, disulphide bridges were detected on insulin fibrillar surfaces⁴².

Another important aspect concerns the electrostatic surface properties of lysozyme fibrils, that play a crucial role in the interaction with external agents. The electrostatic properties are mainly determined by amino acids with charged residues, namely amines and carboxylic groups. Lysozyme is one of the proteins with the highest isoelectric point occurring at pH 11.3^{31,43}. Due to the protonation of most amine groups in the fibrillation at pH 2, it has a clearly positive net charge.

A relevant amount of protonated amine groups (NH_3^+) can be identified in the spectra in Fig. 3 by their rocking vibrational mode at $1144\text{--}1180\text{ cm}^{-1}$ ³⁶. In the sequence of lysozyme, this charged group is present in arginine (Arg), lysine (Lys), asparagine (Asn) and glutamine (Gln). Asn and Gln can be identified from their amino group related vibration modes at 1060 cm^{-1} and 1135 cm^{-1} . Due to their structural similarity these amino acids cannot be further discerned in the spectra. Instead, Arg and Lys residues can be identified by the combination of two bands, as proposed in a previous work²³. Specifically, the concomitant appearance of bands at 1070 cm^{-1} and 1150 cm^{-1} is attributed to Lys, while bands at 1090 cm^{-1} and 1170 cm^{-1} are attributed to Arg. This allows for calculating the propensity of Arg and Lys to 27% and 68%, respectively.

The spectral markers at 1700 cm^{-1} of protonated carboxyl groups⁴², which are present in the side chains of aspartic (Asp) and glutamic (Glu) acids, were found only in the 15% of the spectra.

Specific bands providing information on the secondary structure of fibrils are the Amide I ($1630\text{--}1680\text{ cm}^{-1}$) and Amide III bands ($1220\text{--}1260\text{ cm}^{-1}$)⁴². From Fig. 3A it is obvious that these bands are not always present in the spectra, hampering a direct determination of the secondary structure. The reasons behind this instability, often observed in enhanced Raman spectroscopies, are still under discussion⁴⁴⁻⁴⁶.

The analysis of the surface composition of lysozyme fibrils demonstrates that among other amino acids, Trp and Cys are the most frequently detected residues. Interestingly, these amino acids are mainly located in the four regions of the protein that have been earlier identified as amyloidogenic⁴⁷. Specifically, these particular parts of the sequence act as nucleation centres and thus trigger fibril formation⁴⁸.

Table 1. Assignment of dominating TERS bands. Greek letters indicate the vibrational modes: ν , stretching; δ , bending; ω , wagging.

Assignment ^{5,23,36,37}	Wavenumber (cm^{-1})
$\nu(\text{S-S})$ Cys	530-550
$\nu(\text{C-S})$ Cys	650-680
indole ring breathing Trp	740-770
ring breathing Tyr	825-855
ring breathing Phe	997-1014
indole ring breathing Trp	1004-1010
$\text{NH}_2/\text{NH}_3^+$	1050-1080
$\text{NH}_2/\text{NH}_3^+$	1144-1180
Amide III	1220-1260
$\nu(\text{C-C})$ indole ring Trp	1332-1335
$\delta(\text{CH})$, $\omega(\text{CH}_2)$	1372-1377
$\delta(\text{CH}_3)$	1475
$\nu(\text{C=C})$ indole ring Trp	1533-1552
Amide I	1630-1680
COOH	1700

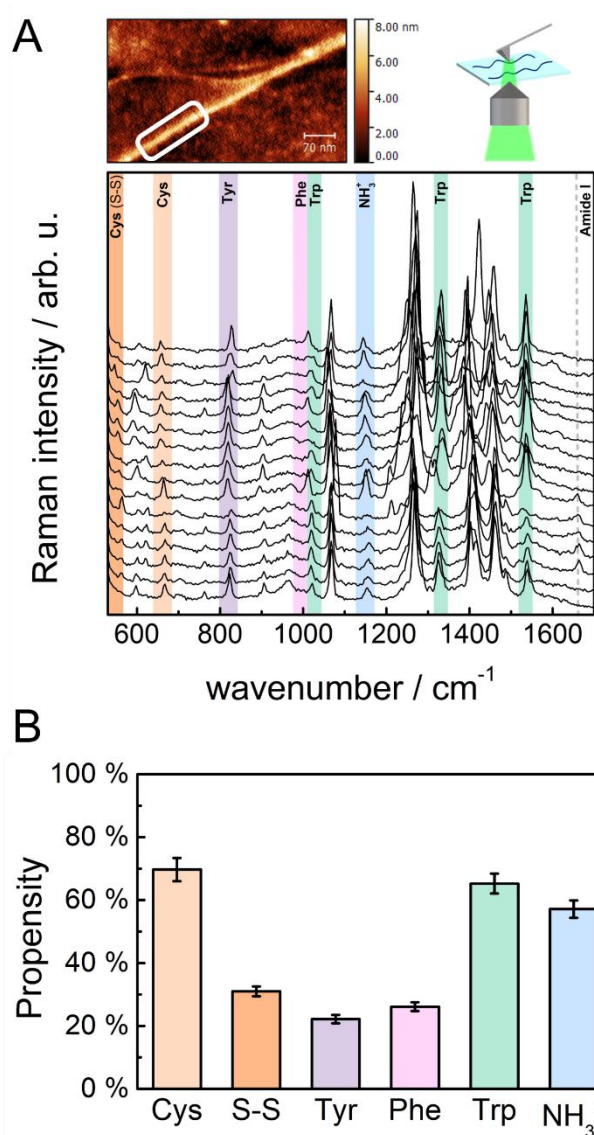


Figure 3. (A) AFM topography image of a single lysozyme fibril and TERS spectra acquired along the same fibril on 2 nm equidistant measurement points. The white box indicates the area where spectra were collected along the fibril main axis. Bands corresponding to the vibrational modes of selected amino acids are highlighted. (B) Propensity of specific amino acids and side groups detected on the surface of mature lysozyme fibrils. The propensity values are calculated from 100 spectra analysed. Columns and bars of the histogram represent the average and standard deviation values obtained for each spectral marker.

Analysis of fibril-gold nanoparticles interaction

The interaction between lysozyme fibrils and AuNPs was analysed by adding 1 μ L of the fibrillar gel to a solution of anionic citrate-capped AuNPs. The extinction spectrum of the sample solution is given in Fig. 4A in comparison to that of the AuNPs stock solution. A clear drop of the absorption of AuNPs at \sim 530 nm, which is accompanied by the onset of a broad shoulder at higher wavelengths, is visible. These spectral changes point to aggregation of AuNPs due to interactions with lysozyme fibrils.

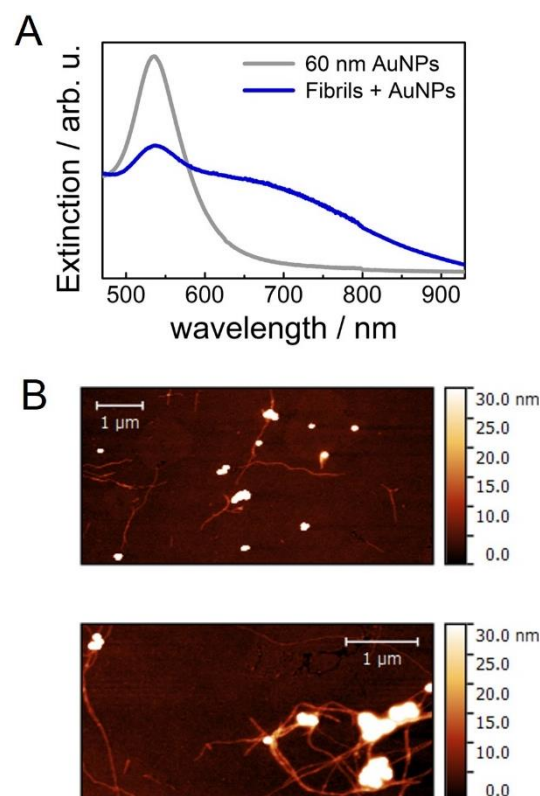


Figure 4. (A) UV-Visible extinction spectra of a AuNPs-fibril sample (blue) and of the 60 nm AuNPs stock solution (grey). (B) Representative topography AFM images of lysozyme fibrils interacting with AuNPs, revealing fibril fragmentation and AuNPs embedded within the fibril network.

To further verify this result and to visualise possible effects on the fibrils morphology, the AuNP-fibril sample was deposited onto a glass slide and the morphology was scanned with an AFM. Representative images of the sample topography are shown in Fig. 4B. The fibrils appear different from those of Fig. 2, specifically they are short fragments with lengths of few micrometres, while clusters of AuNPs appear mainly embedded within networks of these fragments. Moreover, in presence of AuNPs only a few amyloid fibrils remain assembled in intertwined structures. Similar effects have been observed for insulin, where fibrils incubated with AuNPs prompted the formation of agglomerates with AuNPs as aggregation centres¹¹. The results demonstrate that AuNPs should be considered as potential fibrillation disrupter.

The underlying interaction mechanisms between fibrils and AuNPs as well as the effect of fibril rupture were studied at the molecular level by combining TERS and SERS analyses. Thus, on one side, information on the variation of the amino acidic surface composition of fibril fragments were obtained and on the other side, the direct identification of the residues involved in the interaction with the gold surface (see the sketch in Fig. 1C) could be identified.

Representative TERS spectra acquired at 532 nm on a fibril fragment distant from AuNPs are given in Fig. 5A together with the AFM topography image of the probed region. A comparison

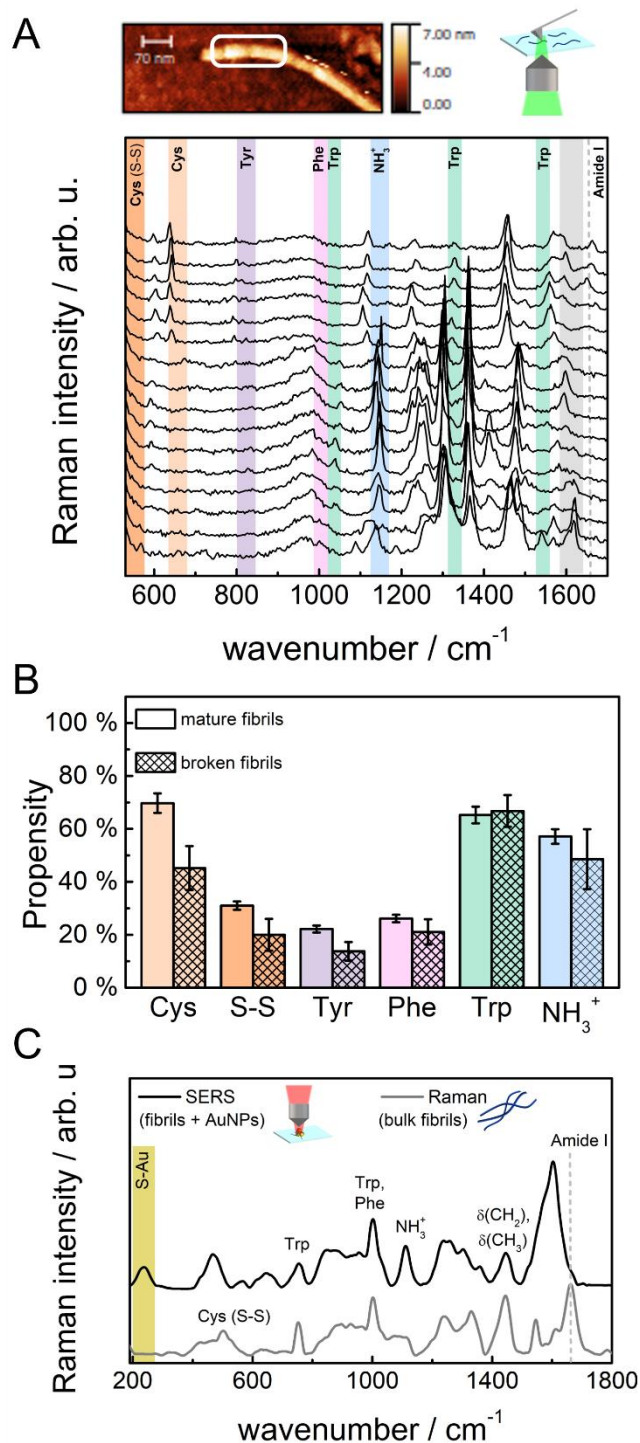


Figure 5. (A) AFM topography image of a single lysozyme fibril fragment generated in the presence of AuNPs and TERS spectra acquired at 532 nm along the same fragment with a 2 nm step size. The white box indicates the area where spectra were collected along the fibril main axis. Bands corresponding to the vibrational modes of selected amino acids are highlighted. (B) Propensity of specific amino acids and functional groups on the surface of fragments, in comparison with those obtained for mature fibrils reported in Figure 3B. The propensity values corresponding to broken fibrils are calculated from 50 spectra analysed. Columns and bars of the histogram represent respectively the average and standard deviation values obtained for each spectral marker. (C) Representative SERS spectrum of fragments of lysozyme fibrils in presence of AuNPs (black) acquired at 633 nm in comparison with the standard Raman spectrum of the lysozyme fibrils (grey).

of the TERS spectra in Figs. 3 and 5 reveals fewer spectral markers of some amino acids, particularly evident in the case of Cys, Tyr and Phe. This might be attributed to a different amino acidic composition of the surface of fibril fragment with respect to intact fibrils. It is assumed that the structural destabilisation of the fibrils was induced by the interaction with AuNPs. As a result, a reorganization of the fibril fragments may occur leading to changes in the surface composition. The observed decrease of selected amino acids and functional groups at the probed surface is given in the histogram of Fig. 5B, where the propensity percentages of fibril fragments are compared with those calculated for intact fibrils (see Fig. 3B). The histogram highlights a clear reduction in the number of Cys after fibril rupture, whose occurrence decreased to 45%. Consequently, the number of S-S bonds in broken fibrils also significantly decreased. A similar trend is also observed for Tyr and Phe presence at the fibrils surface, while the propensity of Trp remains almost unchanged. The presence of amino groups seems to be not markedly affected by the morphological changes of the fibrils, indicating that the positive surface charge is preserved on fibrils fragments.

A representative SERS spectrum recorded at 633 nm is shown in Fig. 5C in comparison to the Raman spectrum of bulk lysozyme fibrils. The bands of the above discussed amino acids are highlighted and assigned. The assignment agrees with that reported in previous contributions^{5,49}. The most relevant spectral feature of the SERS spectrum, that provides insight into the interactions between fibrils and AuNPs, is the presence of a broad peak in the low frequency region at ~230 cm⁻¹, corresponding to the S-Au stretching vibration^{50,51}. This spectral marker points to the formation of a chemical bond between the sulphur atom of Cys in lysozyme and the AuNPs. This result confirms that fibril fragmentation was initiated by the attachment of the sulphur-containing part of the lysozyme to the gold nanoparticles. Thus, the disulphide bridge was broken, as indicated by the decreasing propensity in the TERS experiments of Fig. 5B.

Similar to the TERS spectra, in the SERS spectrum, no Amide I band around 1650 cm⁻¹ was detected. The intense band around 1600 cm⁻¹ can be assigned to the asymmetric carboxylate stretching vibration of the citrate molecules forming the capping of the AuNPs⁵²⁻⁵⁴. This band is also detected in the control SERS spectrum reported in Fig. S2 of the Supporting Information. Notably, the same bands are also present in some of the TERS spectra of fibril fragments (panel A of Fig. 5, highlighted by the grey stripe), while they are completely absent in those of intact fibrils (Fig. 3A). This observation points to the presence of citrate anions on the surface of fibrils fragment that are not in direct contact with AuNPs. During the formation of the S-Au bonds between Cys and AuNPs, the citrate molecules were released from the gold surface. The negatively charged citrate molecules can interact with the positively charged residues of lysozyme. As a result, the stability of the β -sheet network is affected and eventually contributes to fibril dissociation⁵⁵.

The combined analysis of the TERS and SERS spectra suggest that mainly the sulphur-rich regions on the fibrils interact with the AuNPs. Thus, a two-step process inducing fibril breakage in the presence of AuNPs can be postulated: firstly, long range electrostatic attractions induce the accumulation of AuNPs clusters on lysozyme fibrils. Subsequently, the high affinity of the sulphur atoms in Cys towards gold triggers the cleavage of the S-S bonds and the formation of S-Au bonds on the AuNPs. Finally, the breaking of the disulphide bridge destabilises the overall structure of lysozyme fibrils, resulting in their fragmentation.

Conclusions

The development of novel strategies to prevent protein fibrillation is of crucial importance to promote the understanding and the treatment of amyloid fibril-related diseases. A promising approach in this field is the employment of biocompatible and inert metallic nanoparticles, that therefore requires a thorough knowledge of the mechanisms of the interaction between nanoparticles and protein fibrils.

In this study, we presented a novel and straightforward nanoscale spectroscopic approach to gain a deeper insight into the effects of AuNPs on lysozyme amyloid fibrils. We provided for the first-time a near-field spectroscopic characterisation of lysozyme fibrils by exploiting the peculiar high spatial resolution of TERS. The surface characterization of lysozyme fibrils was achieved with an accuracy of a few nanometres, which allowed a preliminary estimation of the abundance of selected amino acids on the fibril surfaces. In addition, the effects induced by the interaction of lysozyme fibrils with AuNPs were investigated by combining scanning probe microscopy with plasmon-enhanced spectroscopies. Our results shed new light on the role of AuNPs in triggering the disassembling and breaking of amyloid structures. The experimental data suggested a significant contribution from Cys-rich regions that preferentially interacted with the AuNPs. As a result, a clear decrease of the abundance of cysteine residues on the surface of broken fibrils was observed. It was postulated that electrostatic interactions and the formation of gold-sulphur covalent bonds played the active roles in the AuNPs induced fibril degradation process.

Our results are encouraging for the development of novel combined diagnostic and therapeutic strategies based on the employment of AuNPs for the treatment of amyloid related diseases. The effects of the size and molecular capping of AuNPs on their ability to disassemble mature fibrils or even prevent fibrillation are important aspects to be investigated at the next stage.

Experimental

Materials

Chicken egg white lysozyme powder was obtained by Sigma Aldrich. Citrate-stabilised gold nanoparticles with a nominal

diameter of 60 nm were provided by Ted Pella Inc. All the chemicals employed in sample preparation were purchased from Sigma-Aldrich and used without further purification.

Lysozyme fibrillation protocol

Lysozyme powder was dissolved to a final concentration of 30 mg/mL in aqueous solution adjusted to pH 2 using HCl. The protein solution was heated at 65°C under continuous and gentle stirring for 48 h. The produced gel was used without further purification. Aliquots of the sample were withdrawn after 2.5 h, 8 h, 24 h and 48 h and diluted (see below) for AFM measurements.

TERS and AFM measurements

For TERS and AFM measurements, an aliquot of 10 µL of the fibril sample were diluted 100 times at pH 2 solution or 1000 times in the gold colloids solution before deposition on a pre-cleaned cover slip. The glass substrates were cleaned with a mixture (ratio 3:1) of concentrated nitric acid and 30 % hydrogen peroxide for 2.5 h. After rinsing with deionized water, the substrates were dried and stored in a desiccator to avoid contamination. 10 µL of the diluted fibril solution were deposited for 5 minutes on the substrate and the solution excess was gently removed by a micropipette.

AFM measurements were performed using the same AFM instrument described in the TERS part by employing silicon AFM probes (Tap190Al-G, Budget Sensors, Germany) with a cantilever with a spring constant of 48 N/m and a tip with nominal radius of curvature lower than 10 nm.

TERS spectra were acquired with AFM probes (Tap190Al-G, Budget Sensors, Germany) evaporated with a 25 nm silver layer forming an island film. An AFM head (Nanowizard III, Bruker-JPK, Germany) was mounted on top of an inverted microscope equipped with a 60× (N.A. 1.45) oil immersion objective. The Raman setup operated in back reflection geometry. Spectra were acquired via grids or lines with a step-size of 2 nm at $\lambda = 532$ nm, $P = 500$ µW, and $t_{acq} = 1$ s.

The spectral analysis was performed on 100 TERS spectra for mature fibrils and on 50 TERS spectra for fibrils fragments, acquired within independent experiments. In the experiments 23 mature fibrils and 20 fibril fragments were probed, employing 7 different TERS tip for each of the two types of samples. AFM images were analysed by Gwyddion software, version 2.52.

UV-Visible extinction spectroscopy

UV-Visible absorbance spectra were collected by employing a double beam UV-Visible spectrophotometer (Cary 60, Agilent Technologies) with a resolution of 1.5 nm in the spectral range 190-1100 nm.

Raman and SERS measurements

Raman and SERS measurements on lysozyme fibrils and on fibrils fragments in interaction with AuNPs were performed by employing a micro-Raman spectrometer (Horiba) in backscattering geometry, equipped with a 633 nm He-Ne laser. A 100× objective (NA=0.9) and a 300 lines/mm diffraction grating were employed for the acquisitions. All the spectra are presented after a polynomial baseline subtraction.

Conflicts of interest

There are no conflicts to declare.

Acknowledgements

AC would like to thank Prof. A. Nucara for useful discussions.

Funding sources

AC acknowledges Sapienza University for funding "Avvio alla Ricerca" project n.AR11816436CE4810 and "Joint Research Projects for the mobility of PhD students". VD acknowledges support by the German Science Foundation DFG via the CRC 1375 NOA – C2 and the Leibniz Science Campus "InfectoOptics" via Project HoTAim 2.0. TDG acknowledges funding via the DFG Project No. 448666227.

References

- 1 F. Chiti and C. M. Dobson, Protein misfolding, functional amyloid, and human disease, *Annual Review of Biochemistry*, 2006, **75**, 333-366.
- 2 P. Arosio, T. P. Knowles and S. Linse, On the lag phase in amyloid fibril formation, *Physical Chemistry Chemical Physics*, 2015, **17** (12), 7606-7618.
- 3 M. Carbonaro, F. Ripanti, A. Filabozzi, V. Minicozzi, F. Stellato, E. Placidi, S. Morante, A. Di Venere, E. Nicolai, P. Postorino and A. Nucara, Human insulin fibrillogenesis in the presence of epigallocatechin gallate and melatonin: structural insights from a biophysical approach, *International Journal of Biological Macromolecules*, 2018, **115**, 1157-1164.
- 4 T. Deckert-Gaudig and V. Deckert, High resolution spectroscopy reveals fibrillation inhibition pathways of insulin, *Scientific Reports*, 2016, **6**, 39622.
- 5 S. Mangialardo, L. Gontrani, F. Leonelli, R. Caminiti and P. Postorino, Role of ionic liquids in protein refolding: native/fibrillar versus treated lysozyme, *RSC Advances* 2012 **2** (32), 12329-12336.
- 6 T. John, A. Gladysz, C. Kubeil, L. L. Martin, H. J. Risselada and B. Abel, Impact of nanoparticles on amyloid peptide and protein aggregation: a review with a focus on gold nanoparticles, *Nanoscale*, 2018, **10** (45), 20894-20913.
- 7 H. R. Barros, M. Kokkinopoulou, I. C. Riegel-Vidotti, K. Landfester and H. Therien-Aubin, Gold nanocolloid-protein interactions and their impact on sheet amyloid fibril formation, *RSC Advances*, 2018, **8** (2), 980-986.
- 8 S. I. Yoo, M. Yang, J. R. Brender, V. Subramanian, K. Sun, N. E. Joo, S.-H. Jeong, A. Ramamoorthy and N. A. Kotov, Inhibition of amyloid peptide fibrillation by inorganic nanoparticles: functional similarities with proteins, *Angewandte Chemie International Edition*, 2011, **50** (22), 5110-5115.
- 9 G. Gao, M. Zhang, D. Gong, R. Chen, X. Hu and T. Sun, The size-effect of gold nanoparticles and nanoclusters in the inhibition of amyloid-fibrillation, *Nanoscale*, 2017, **9** (12), 4107-4113.
- 10 G. Brancolini, D. Toroz and S. Corni, Can small hydrophobic gold nanoparticles inhibit β 2-microglobulin fibrillation?, *Nanoscale*, 2014, **6** (14), 7903-7911.
- 11 S. Hsieh, C. Chang and H. Chou, Gold nanoparticles as amyloid-like fibrillogenesis inhibitors, *Colloids and Surfaces B: Biointerfaces*, 2013, **112**, 525-529.
- 12 L. Fei and S. Perrett, Effect of nanoparticles on protein folding and fibrillogenesis, *International Journal of Molecular Sciences*, 2009, **10** (2), 646-655.
- 13 M. Barbalinardo, A. Antosova, M. Gambucci, Z. Bednarikova, C. Albonetti, F. Valle, P. Sassi, L. Latterini, Z. Gazova and E. Bystrenova, Effect of metallic nanoparticles on amyloid fibrils and their influence to neural cell toxicity, *Nano Research*, 2020, **13** (4), 1081-1089.
- 14 D. K. Ban and S. Paul, Functionalized gold and silver nanoparticles modulate amyloid fibrillation, defibrillation and cytotoxicity of lysozyme via altering protein surface character, *Applied Surface Science* 2019, **473**, 373-385.
- 15 Y.-H. Liao, Y.-J. Chang, Y. Yoshiike, Y.-C. Chang and Y.-R. Chen, Negatively charged gold nanoparticles inhibit Alzheimer's amyloid- fibrillization, induce fibril dissociation, and mitigate neurotoxicity, *Small*, 2012, **8** (23), 3631-3639.
- 16 J. Langer, D. Jimenez de Aberasturi, J. Aizpurua, R. A. Alvarez-Puebla, B. Auguie, J. J. Baumberg, G. C. Bazan, S. E. Bell, A. Boisen, A. G. Brolo, *et al.*, Present and future of surface-enhanced Raman scattering, *ACS Nano*, 2019, **14**(1), 28-117.
- 17 M. I. Stockman, K. Kneipp, S. I. Bozhevolnyi, S. Saha, A. Dutta, J. Ndukaife, N. Kinsey, H. Reddy, U. Guler, V. M. Shalae, *et al.*, Roadmap on plasmonics, *Journal of Optics*, 2018, **20** (4), 043001.
- 18 D. Cialla-May, X.-S. Zheng, K. Weber and J. Popp, Recent progress in surface-enhanced Raman spectroscopy for biological and biomedical applications: from cells to clinics, *Chemical Society Reviews*, 2017, **46** (13), 3945-3961.
- 19 P. Verma, Tip-enhanced Raman spectroscopy: technique and recent advances, *Chemical Reviews*, 2017, **117** (9), 6447-6466.
- 20 A. B. Zrimsek, N. Chiang, M. Mattei, S. Zaleski, M.O. McAnally, C. T. Chapman, A. Henry, G. C. Schatz and R. P. Van Duyne, Single-molecule chemistry with surface-and tip-enhanced Raman spectroscopy, *Chemical Reviews*, 2017, **117** (11), 7583-7613.
- 21 T. Deckert-Gaudig, A. Taguchi, S. Kawata and V. Deckert, Tip-enhanced Raman spectroscopy-from early developments to recent advances, *Chemical Society Reviews*, 2017, **46**(13), 4077-4110.
- 22 R. M. Stöckle, Y. D. Suh, V. Deckert and R. Zenobi, Nanoscale chemical analysis by tip-enhanced Raman spectroscopy, *Chemical Physics Letters*, 2000, **318** (1-3), 131-136.
- 23 T. Deckert-Gaudig, D. Kurouski, M. A. Hedegaard, P. Singh, I. K. Lednev and V. Deckert, Spatially resolved spectroscopic differentiation of hydrophilic and hydrophobic domains on individual insulin amyloid fibrils, *Scientific Reports* 2016, **6**, 33575.
- 24 C. D'Andrea, A. Foti, M. Cottat, M. Banchelli, C. Capitini, F. Barreca, C. Canale, M. de Angelis, A. Relini, O. M. Marago, R. Pini, F. Chiti, P. G. Gucciardi and P. Matteini, Nanoscale discrimination between toxic and nontoxic protein misfolded oligomers with tip-enhanced Raman spectroscopy, *Small*, 2018, **14** (36), 1800890.
- 25 Z. He, Z. Han, M. Kizer, R. J. Linhardt, X. Wang, A. M. Sinyukov, J. Wang, V. Deckert, A. V. Sokolov, J. Hu and M. O. Scully, Tip-

- enhanced Raman imaging of single stranded DNA with single base resolution, *Journal of the American Chemical Society*, 2019, **141** (2), 753-757.
- 26 Z. He, W. Qiu, M. E. Kizer, J. Wang, W. Chen, A. V. Sokolov, X. Wang, J. Hu, M and O. Scully, Resolving the Sequence of RNA Strands by Tip-Enhanced Raman Spectroscopy, *ACS Photonics*, 2021, **8** (2) 424–430.
- 27 R. Swaminathan, V. K. Ravi, S. Kumar, M. V. S. Kumar and N. Chandra, Lysozyme: a model protein for amyloid research, in: *Advances in Protein Chemistry and Structural Biology* 2011 **84**, 63-111.
- 28 L. N. Arnaudov and R. de Vries, Thermally induced fibrillar aggregation of hen egg white lysozyme, *Biophysical Journal*, 2005, **88** (1), 515-526.
- 29 V. A. Shashilov and I. K. Lednev, 2D correlation deep UV resonance Raman spectroscopy of early events of lysozyme fibrillation: kinetic mechanism and potential interpretation pitfalls, *Journal of the American Chemical Society*, 2008, **130** (1), 309-317.
- 30 C. Fasolato, S. Giantulli, A. Capocefalo, Y. Tournia, D. Notariello, F. Mazzarda, I. Silvestri, P. Postorino and F. Domenici, Antifolate SERS-active nanovectors: quantitative drug nanostructuring and selective cell targeting for effective theranostics, *Nanoscale*, 2019, **11** (32), 15224-15233.
- 31 F. Brasili, A. Capocefalo, D. Palmieri, F. Capitani, E. Chiessi, G. Paradossi, F. Bordini and F. Domenici, Assembling patchy plasmonic nanoparticles with aggregation dependent antibacterial activity, *Journal of Colloid and Interface Science*, 2020, **580**, 419-428.
- 32 J. Kneipp, Interrogating cells, tissues, and live animals with new generations of surface-enhanced Raman scattering probes and labels, *ACS Nano*, 2017, **11** (2), 1136-1141.
- 33 S. E. Hill, J. Robinson, G. Matthews and M. Muschol, Amyloid protofibrils of lysozyme nucleate and grow via oligomer fusion, *Biophysical Journal*, 2009, **96** (9), 3781-3790.
- 34 J. Adamcik and R. Mezzenga, Study of amyloid fibrils via atomic force microscopy, *Current Opinion in Colloid & Interface Science*, 2012, **17** (6), 369-376.
- 35 C. Lara, I. Usov, J. Adamcik and R. Mezzenga, Sub-persistence-length complex scaling behavior in lysozyme amyloid fibrils, *Physical Review Letters*, 2011, **107** (23), 238101.
- 36 S. Bonhommeau and S. Lecomte, Tip-enhanced Raman spectroscopy: A tool for nanoscale chemical and structural characterization of biomolecules, *ChemPhysChem*, 2018, **19** (1), 8-18.
- 37 T. Deckert-Gaudig, E. Rauls and V. Deckert, Aromatic amino acid monolayers sandwiched between gold and silver: a combined tip-enhanced Raman and theoretical approach, *The Journal of Physical Chemistry C*, 2009, **114** (16), 7412-7420.
- 38 R. E. Caneld, The amino acid sequence of egg white lysozyme, *Journal of Biological Chemistry* 1963, **238** (8), 2698-2707.
- 39 B. Guilherme daFonseca, L. A. S. Costa and A. C. Sant'Ana, Insights of adsorption mechanisms of trppeptides on plasmonic surfaces by SERS, *Spectrochimica Acta Part A: Molecular and Biomolecular Spectroscopy*, 2018, **190**, 383-391.
- 40 D. Kourouski, R. P. Van Duyne and I. K. Lednev, Exploring the structure and formation mechanism of amyloid fibrils by Raman spectroscopy: a review, *Analyst*, 2015, **140** (15), 4967-4980.
- 41 S. S.-S.Wang, K.-N. Liu and B.-W.Wang, Effects of dithiothreitol on the amyloid fibrillogenesis of hen egg-white lysozyme, *European Biophysics Journal*, 2010, **39** (8), 1229-1242.
- 42 D. Kourouski, T. Deckert-Gaudig, V. Deckert and I. K. Lednev, Structure and composition of insulin fibril surfaces probed by TERS, *Journal of the American Chemical Society*, 2012, **134** (32), 13323-13329.
- 43 L. Wetter and H. Deutsch, Immunological studies on egg white proteins, *Journal of Biological Chemistry*, 1951, **192**, 237-242.
- 44 D. Kourouski, T. Postiglione, T. Deckert-Gaudig, V. Deckert, I. K. Lednev, Amide I vibrational mode suppression in surface (SERS) and tip (TERS) enhanced Raman spectra of protein specimens, *Analyst*, 2013, **138** (6), 1665-1673.
- 45 C. Blum, T. Schmid, L. Opilik, N. Metanis, S. Weidmann and R. Zenobi, Missing amide I mode in gap-mode tip-enhanced Raman spectra of proteins, *The Journal of Physical Chemistry C*, 2012, **116** (43), 23061-23066.
- 46 S. Sloan-Dennison, C. M. Zoltowski, P. Z. El-Khoury, and Z. D. Schultz, Surface Enhanced Raman Scattering Selectivity in Proteins Arises from Electron Capture and Resonant Enhancement of Radical Species, *The Journal of Physical Chemistry C*, 2020, **124** (17), 9548-9558.
- 47 G. G. Tartaglia, A. P. Pawar, S. Campioni, C. M. Dobson, F. Chiti and M. Vendruscolo, Prediction of aggregation-prone regions in structured proteins, *Journal of Molecular Biology*, 2008, **380** (2), 425-436.
- 48 V. Castillo and S. Ventura, Amyloidogenic regions and interaction surfaces overlap in globular proteins related to conformational diseases, *PLoS Computational Biology*, 2009, **5** (8), e1000476.
- 49 B. Fazio, C. D'Andrea, A. Foti, E. Messina, A. Irrera, M. G. Donato, V. Villari, N. Micali, O. M. Maragò and P. G. Gucciardi, SERS detection of Biomolecules at Physiological pH via aggregation of Gold Nanorods mediated by Optical Forces and Plasmonic Heating, *Scientific Reports*, 2016, **6** (1), 1-13.
- 50 B. Varnholt, P. Oulevey, S. Lubert, C. Kumara, A. Dass and T. Burgi, Structural information on the Au-S interface of thiolate-protected gold clusters: a Raman spectroscopy study, *The Journal of Physical Chemistry C*, 2014, **118** (18), 9604-9611.
- 51 A. Capocefalo, D. Mammucari, F. Brasili, C. Fasolato, F. Bordini, P. Postorino and F. Domenici, Exploring the potentiality of a SERS-active pH nano-biosensor, *Frontiers in Chemistry*, 2019, **7**:413.
- 52 D. B. Gryns, B. de Nijs, A. R. Salmon, J. Huang, W. Wang, W. H. Chen, O. A. Scherman and J. J. Baumberg, Citrate Coordination and Bridging of Gold Nanoparticles: The Role of Gold Adatoms in AuNP Aging, *ACS Nano*, 2020, **14** (7), 8689-8696.
- 53 D. Caprara, F. Ripanti, A. Capocefalo, A. Sarra, F. Brasili, C. Petrillo, C. Fasolato and P. Postorino, DNA functionalized gold nanoparticle assemblies for surface enhanced Raman scattering, *Colloids and Surfaces A: Physicochemical and Engineering Aspects*, 2020, **589**, 124399.
- 54 Y. Zhang, F. Wang, H. Yin and M. Hong, Nonuniform distribution of capping ligands promoting aggregation of silver nanoparticles for use as a substrate for SERS, *Advances in Nanoparticles*, 2013, **2** (02), 104.
- 55 S. L. Shammas, T. P. Knowles, A. J. Baldwin, C. E. MacPhee, M. E. Welland, C. M. Dobson and G. L. Devlin, Perturbation of the stability of amyloid fibrils through alteration of electrostatic interactions, *Biophysical Journal*, 2011, **100** (11), 2783-2791.